Materials Research. 2023; 26:e20230230
DOI: https://doi.org/10.1590/1980-5373-MR-2023-0230

Nanostructured Powders of AA7075 - SiC Manufactured by High-Energy Ball Milling in a Bath of Isopropyl Alcohol

Wésia Amanda de Oliveira Barbosa[a], Euclides Apolinário Cabral de Pina[b], Alexandre Douglas Araújo de Moura[b], Pilar Rey Rodrigues[c], Oscar Olímpio de Araújo Filho[d], Ivanilda Ramos de Melo[d], Heronilton Mendes de Lira[a]*

[a]Universidade Federal Rural de Pernambuco, Unidade Acadêmica de Belo Jardim, Belo Jardim, PE, Brasil.
[b]Universidade Federal Rural de Pernambuco, Unidade Acadêmica do Cabo de Santo Agostinho, Cabo de Santo Agostinho, PE, Brasil.
[c]AIMEN Technology Centre, Relva 27A-Torneiros, 36410 Porriño-Pontevedra, Spain.
[d]Universidade Federal de Pernambuco, Recife, PE, Brazil.

Received: May 8, 2023; Revised: August 23, 2023; Accepted: October 20, 2023

In this study, aluminum alloy 7075 (AA7075) nanopowders were prepared by High-Energy Ball Milling (HEBM) in a bath of isopropyl alcohol. The process was investigated in different milling times and silicon carbides (SiC) reinforcement percentual. The effects of these parameters on the samples were characterized by X-ray diffraction (XRD), Laser Diffraction (LD), Scanning Electron Microscopy (SEM), and Energy Dispersive Spectroscopy (EDS). The XRD analyses showed that as the grinding time increases, the micro deformation also increases, while the crystallite and particle size decrease until a constant value at 480 min. If the percentual of SiC reinforcement increases until 5 percent, there is a minimum change in the results compared to AA 7075 milling 480 min with no reinforcement. On the other hand, when the AA7075 was milled for 480 min and reinforced by 10 percent SiC, the best structural refinement result was achieved.

Keywords: *Nanostructured Al Powder, High-Energy Ball Milling, Powder Metallurgy.*

1. Introduction

The growing demand for aluminum in aerospace sectors has spurred research into enhancing the reinforcement of aluminum metal matrices across technological uses. The aim is to substitute traditional materials and their alloys with improved alternatives. Aluminum metal matrices reinforced with other materials exhibit high mechanical and tribological properties and an attractive strength-to-weight ratio[1-7]. In this context, aluminum alloy 7075 (AA7075) as a matrix is notable for its low density and good workability, offering a favorable combination of strength, ductility, and toughness. On the other hand, introducing Silicon Carbide (SiC) as reinforcement, whether in micron or nanoscale form, enhances wear resistance and hardness due to its low density and high strength[8-15].

Furthermore, attempts were made to explore severe plastic deformation processes to obtain nanostructured materials[16-19]. Among these mechanical methods, High-Energy Ball Milling (HEBM) is a simple and efficient technique to prepare alloys at room temperature with nanocrystalline grains (measuring below 100nm)[20-23].

HEBM is characterized by the repeated flattened, cold-welded, fractured, and rewelded welding of powder particles under different conditions until the rate of fracturing is achieved. It introduces shear bands that contain a high-density network of dislocations and other crystallite defects that reduce crystallite size and particle size and promote changes in morphology up to reach the equilibrium state[24-26]. In this phase, the segregation effects decrease, and a homogeneous distribution of reinforcement into the particles can be obtained[27].

The responses obtained by HEBM depend on the type of mill and the process variables, being the most typically studied: milling time, rotation speed, ball-to-powder ratio, and reinforcement percentual, among others[28-31]. However, when the HEBM occurs in a liquid medium, the environment can influence the results[32,33]. It has been reported that wet grinding is a more suitable method than dry grinding to obtain finer-ground products because the solvent molecules are adsorbed on the newly formed surfaces of the particles and lower their surface energy. The less-agglomerated condition of the powder particles in the wet medium is also a helpful factor[34,35]. Besides that, as a disadvantage, the rate of amorphization and the increase of the contamination of the process is faster during wet grinding than during dry grinding[36-38]. The critical issue arises from the contribution of the influence of the liquid on the resulting grain and particle/morphology size.

The main aim of the research presented here was to investigate the effect of changing milling time and reinforced percentual of SiC applied to AA7075 manufactured by high-energy ball milling in a liquid media of isopropyl alcohol to obtain nanocrystalline powders.

*e-mail: heronilton.lira@ufrpe.br

2. Experimental Procedure

Commercial gas-atomized nanocrystalline powder AA7075 from Aluminum Powder Corporate and nanometric powder of SiC, with a particle size D (50) 50nm, supplied by Iolitec GMBH, were used as matrices and reinforcement, respectively. In Table 1, the chemical composition of AA7075 is shown[39].

The materials, matrix, and reinforcement were deposited into a stainless-steel attrition ball mill equipped with a K-type thermocouple and a temperature controller. Milling was carried out at 900 rpm with balls 100C6 (1%C, 1,5%Cr) of 6,4mm and balls to powder mass ratio of 20:1. For each sample, 50g of material was manufactured at a bath of 100ml isopropyl alcohol (C3H7OH - 99,82%) and 1wt% of zinc stearate (C36H70O4Zn) was used as process control agent (PCA). The process temperature of 25ºC was maintained via a jacket refrigerated with water around the attritor mill[40]. The following milling conditions were studied:

a) Milling time: 60, 120, 240, and 480 minutes.
b) Reinforce weight percentual (SiC): 1wt%, 2wt%, 5wt%, and 10wt%.

After gridding, the samples were dried at 100ºC to evaporate the residues. The effects of crystallite size, micro deformation, particle size, morphology, and chemical composition were analyzed.

The crystallite size and micro deformation were investigated by X-ray diffraction, XRD (Rigaku Ultima III) in the range of 5-120º with a step rate of 0.02º/s at 40kV and 30mA. The Match Phase Analyses software was used to identify the phases and to index the diffraction peaks.

Utilizing the linear regression analysis of the Williamson – Hall plot equation (Equation 1)[41,42], the determination of crystallite size and the assessment of micro deformation to the Full Width at Half Maximum (FWHM) of the peak were conducted for the four principal aluminum peaks, with a confidence level exceeding 92 percent. Comparatively, the instrument effect on crystallite size was not considered.

$$FWHM = k\lambda / L\cos\theta + 4\varepsilon \, tag\theta \quad (1)$$

where "FWHM" is the full width at half maximum in radians; "k" is a constant (0.94); "λ" is the wavelength of the x-rays (15.4nm); "L" is the average crystallite size; "θ" is the Bragg angle, and "ε" is the micro deformation measured.

The particle size was determined by Laser Diffraction (Malvern Mastersizer 2000), where the sample was suspended in water and agitated by ultrasound to size range 0.02μm to 2000μm[43].

The laser beam incident by an ensemble of particles dispersed in either a liquid or an air stream promotes light scattering, and the particle size is calculated as spheres of equal volume. The scattering or diffraction angles exhibit distinct traits related to particle size, as they progressively decrease with an increase in particle size. The equations for the average and uncertain of particle sizes assume the size distribution is available as a histogram. The measure D (0.5) represents the median particle diameter corresponding to the 50th percentile of the cumulative undersize distribution[44-46].

Lastly, the morphology and composition of the particle were analyzed by Scanning Electron Microscopy (Hitachi TM 3000) operating at 20kV, equipped with an EDX probe.

3. Results and Discussion

The results of eight samples compare the AA7075 as-received, AA7075 as a function of milling time, and AA7075 as a function of SiC reinforce percentual.

Figure 1 presents the morphology and alloy elements detected by EDS microanalysis of AA7075 starting powder. Table 2 shows all values found to the crystallite size, micro deformation, and particle size.

Table 1. Chemical Composition AA 7075.

Material	Al	Cr	Cu	Fe (max)	Mg	Mn (max)	Si (max)	Ti (max)	Zn
Weight %	87.1-91.4	0.18- 0.28	1.2-2.0	0.5	2.1-2.9	0.3	0.4	0.2	5.1-6.1

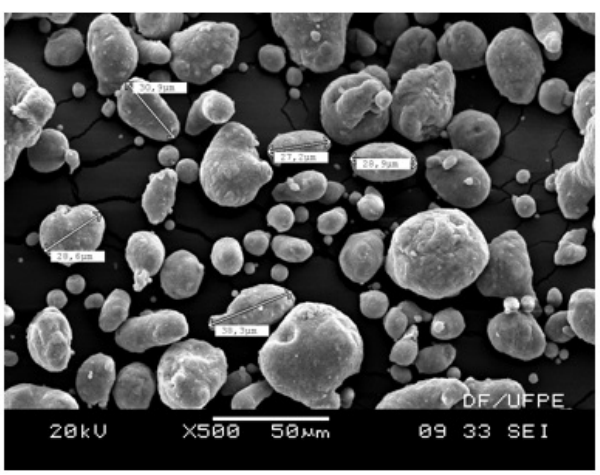

EDS AA7075 As Received		
Element	**Weight (%)**	**Error**
Aluminum	88.70	±3.5
Oxygen	3.73	±0.7
Magnesium	2.20	±0.1
Zinc	3.85	±0.1
Copper	1.52	±0.1

Figure 1. SEM AA7075 as received (x500) and EDS microanalysis.

Table 2. Values of crystallite size, micro deformation, and particle size for all samples AA7075.

Sample Number	Crystallite Size [nm]	Micro Deformation [%]	Particle Size D (0.5) [µm]	Milling Time [min]	Reinforce (SiC) [wt%]
AA075	49	0.02	31.71	As Received	
1	33	0.06	37.62	60	0
2	32	0.06	25.44	120	0
3	30	0.10	16.28	240	0
4	29	0.12	10.64	480	0
5	29	0.12	11.18	480	1
6	32	0.10	13.66	480	2
7	29	0.12	10.80	480	5
8	25	0.16	9.04	480	10

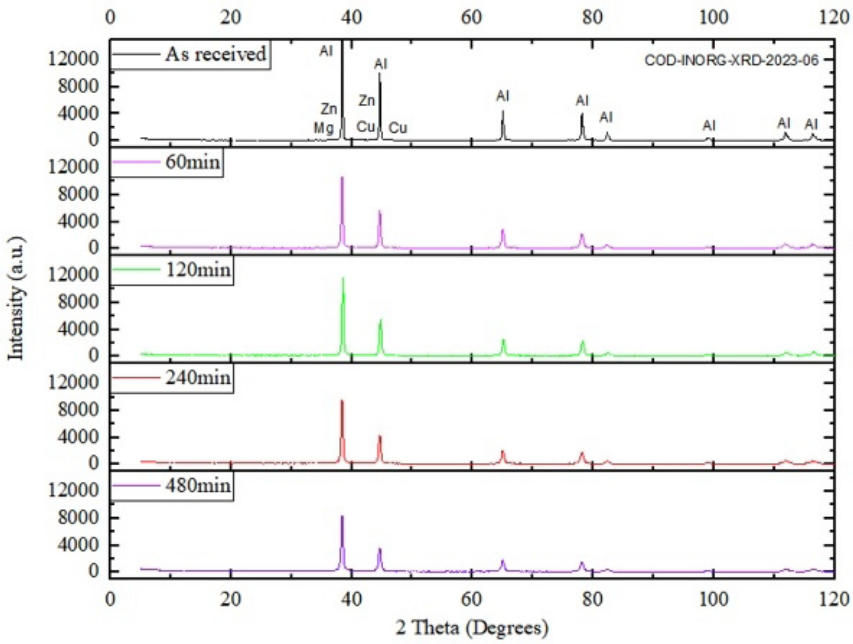

Figure 2. Standard of X-rays diffraction AA7075 as a function of the milling time.

The AA7075 as-received powder was round because of its production process[44-46]. Some particle sizes presented values around 30µm, according to particle size measured by Laser Diffraction D (0.5) 31.71µm. Besides that, the crystallite sizes and micro deformation measured 49nm and 0,02 percent, respectively.

3.1. AA7075 as a function of milling time

Figures 2-5 present, at the sequence, the graphs of X-rays diffraction, particle size distribution, crystallite size, micro deformation, and particle size, particle morphologies, and AA7075 milled 480 min EDS as a function of the milling time.

The values obtained to crystallite size standard agree with the particle size distribution and micro deformation.

Table 2 and Figure 4 present the internal structures refinement as a function logarithmic of milling time. The crystallite size decreased from 49nm to about 30nm while the micro deformation increased from 0.02 percent to around 0.12 percent. It is evidenced by diffraction peaks that became wider, smaller, and not shifted. The X-rays are reflected in a diffraction peak when a crystalline material is struck. However, the effects that lead to an increase in its width and a subsequent decrease in intensity are attributed to the reduction of crystallite size and increased micro deformation[47-49].

Furthermore, Table 2 and Figure 3 show particle size decreased from about D(50) 30µm to the value constant D(50) 10µm in 480 min. Until 240 minutes of milling, there is an indication of competition between cold welding and fracturing because the particles are still flattened, and at 480 min, the fracture domain is observed[50-52] (Figure 5). Various mechanical factors and parameters, including wet milling and energetic conditions, have influenced this response. Wet milling contributed to the formation of good-proportion particles. The high-energy collision among the milling balls played a crucial role in uniformly dispersing the stress in the matrix[53-55].

Finally, AA 7075 milled 480 min EDS (Figure 5) reveals no contamination traces from the steel balls or the stainless steel attritor mill were detected. The presence of liquid alcohol in the milling process increased the oxygen percentage in the sample.

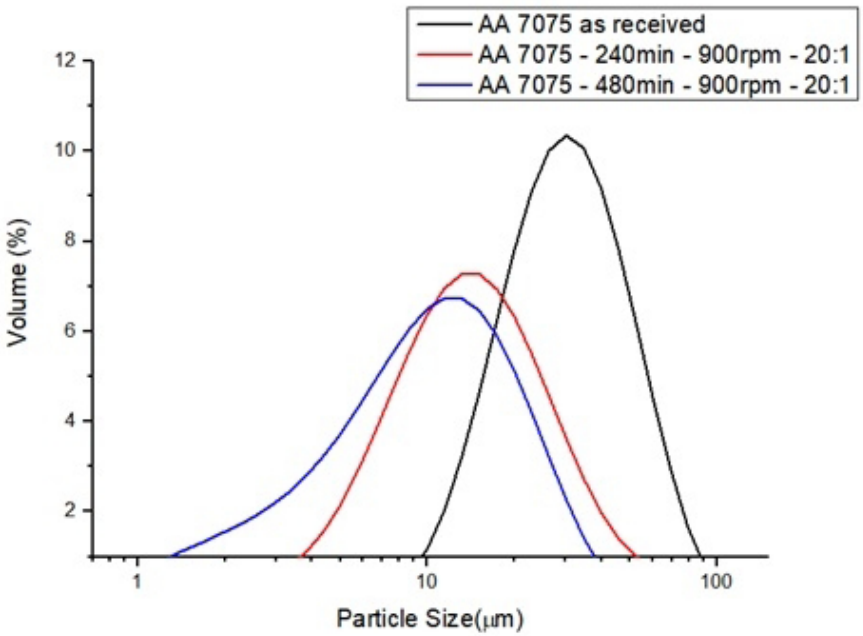

Figure 3. Particle size distribution AA 7075 as a function of the milling time.

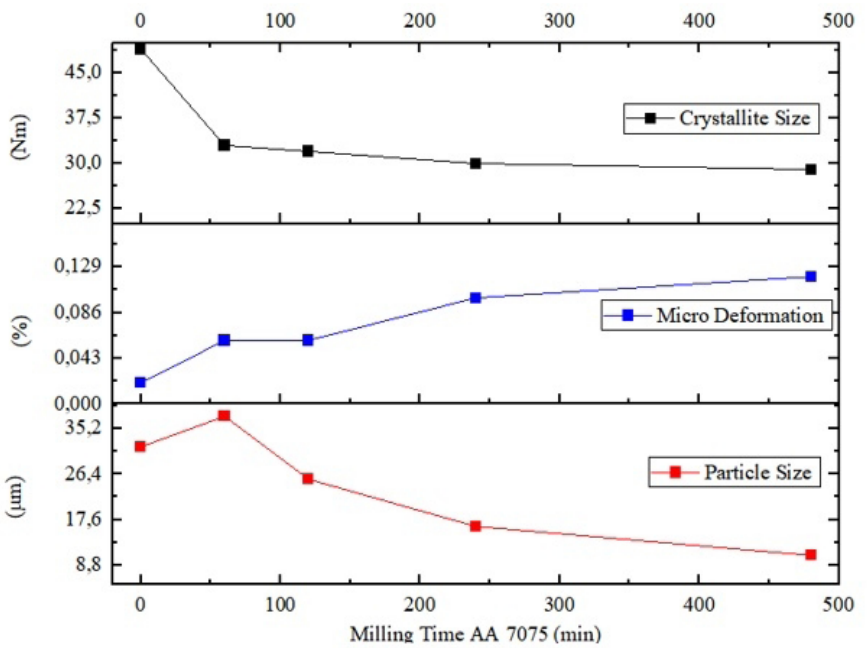

Figure 4. Crystallite size, micro deformation, and particle size of AA 7075 as a function of the milling time.

3.2. AA7075 as a function of SiC reinforce percentual.

In its turn, Figures 6-9 show the standard of X-rays diffraction, particle size distribution, crystallite size, micro deformation, particle size, particle morphologies, and AA7075 milled 480 min + 10% SiC EDS as a function of SiC reinforcement percentual.

The crystallite size, micro deformation, particle size, morphologies, and chemical composition present similar to values found in AA7075 milled 480 min, independently if no reinforcement was used or if the SiC reinforces percentual was used until 5 percent due to the AA7075 can support high-stress structurals[56]. Significant changes were observed when 10 percent of SiC reinforcement was applied; in this condition, the best refinement structural results were achieved: 25nm of crystallite size, 0.16 percent of micro deformation, and 9μm of particle size.

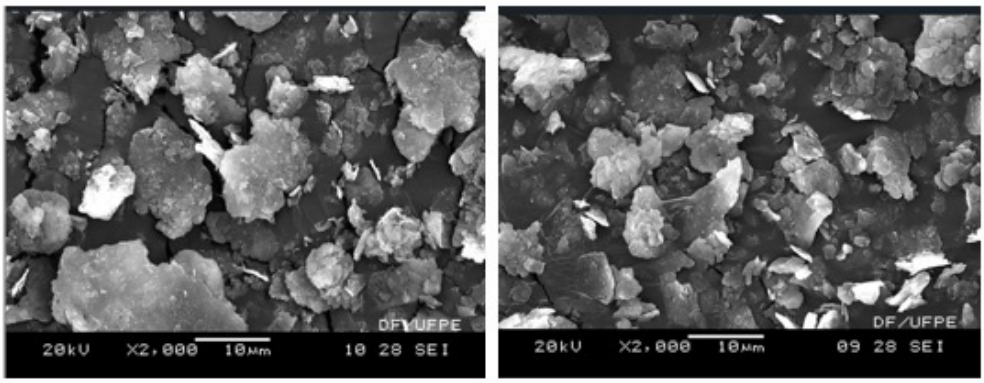

a) b)

EDS AA 7075 Milled 480 min		
Element	**Weight (%)**	**Error**
Aluminum	70.78	±3.8
Oxygen	21.76	±0.9
Magnesium	2.11	±0.1
Zinc	3.86	±0.1
Copper	1.49	±0.1

Figure 5. SEM AA7075 as a function of the milling time (2000x): a) 240min e b) 480min and EDS AA7075 milled 480 min.

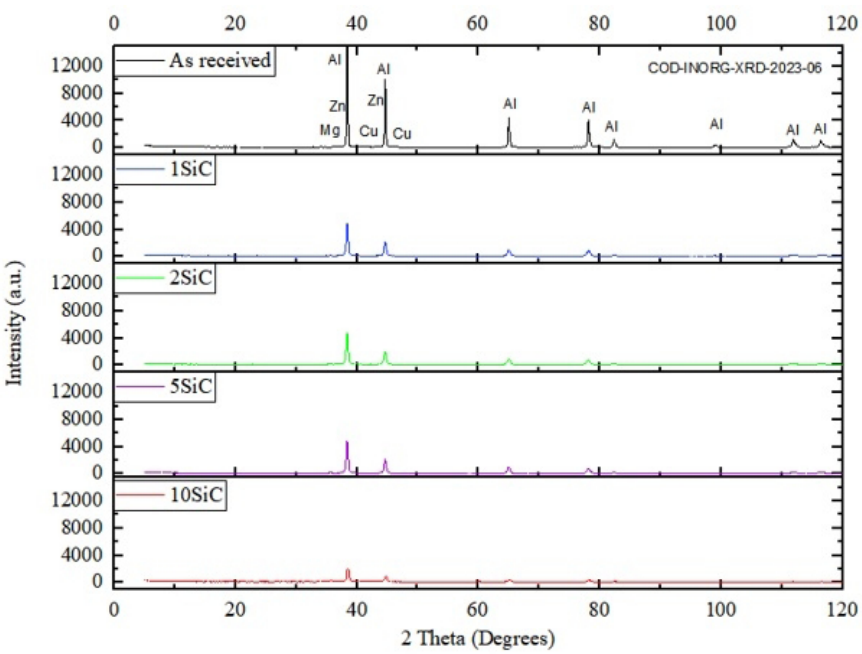

Figure 6. Standard of X-rays diffraction as a function of SiC reinforce percentual.

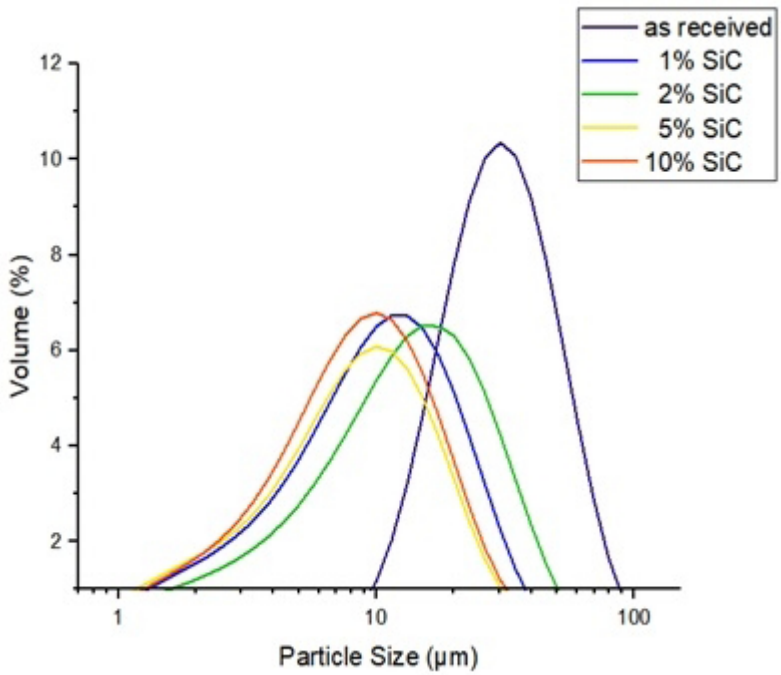

Figure 7. Particle size distribution AA 7075 as a function of SiC reinforce percentual.

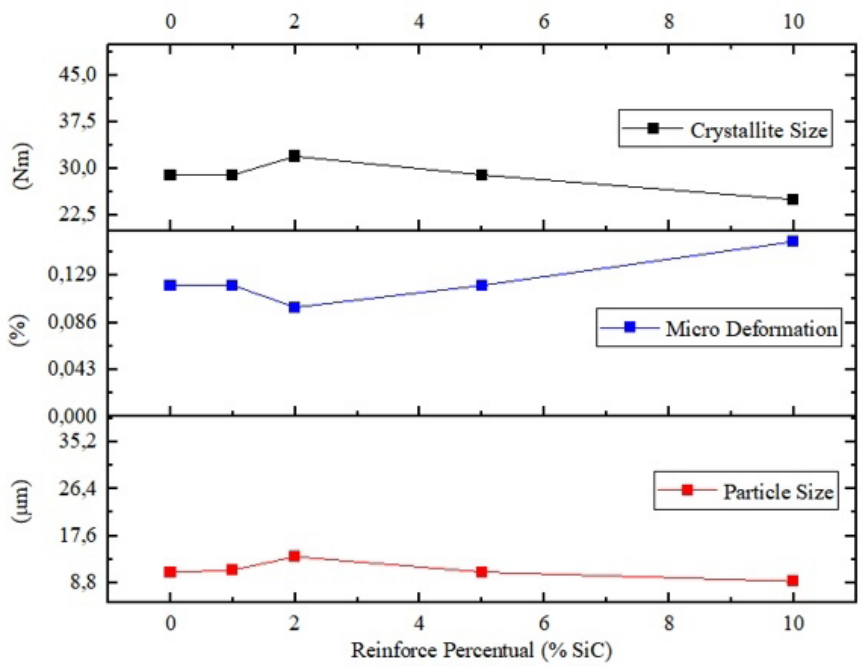

Figure 8. Crystallite size, micro deformation, and particle size of AA 7075 as a function of SiC reinforce percentual.

4. Conclusions

Nanosize powders of AA7075 were manufactured by high-energy ball milling, and the milling time and SiC reinforce percentual were studied. The following results can be resumed according to below:

1- For AA7075 as a function of milling time, the crystallite size and particle size decrease from 49nm up to about 30nm and from D (50) 30µm to D (50) 10µm, respectively, while the micro deformation increases from 0.02 percent to around 0.12 percent to a constant value of 480 minutes.

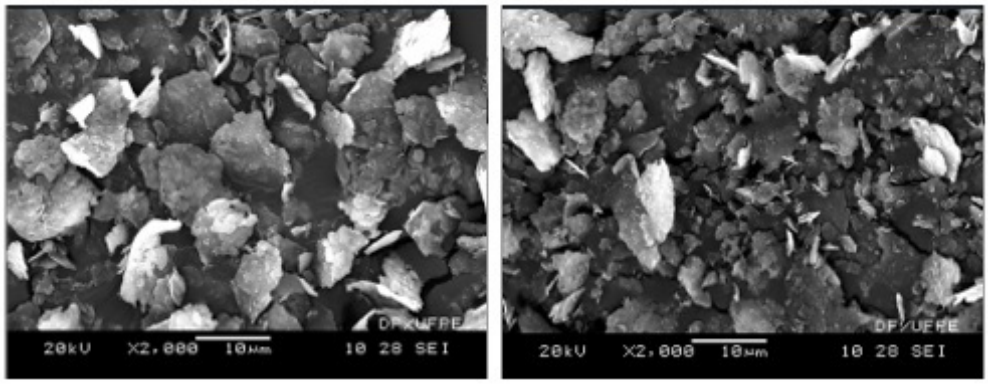

a) b)

EDS AA7075 Milled 480 min + 10%SiC		
Element	Weight (%)	Error
Aluminum	71.59	±.2.6
Oxygen	20.57	±0.8
Magnesium	2.04	±0.1
Zinc	2.51	±0.1
Copper	1.20	±0.1
Silicon	2.09	±0.1

Figure 9. SEM AA7075 as a function of reinforce percentual (2000x): a)5% SiC e b)10% SiC and EDS AA7075 Milled 480 min + 10% SiC.

2- The presence of liquid alcohol in the milling process increased the oxygen percentage in the sample.
3- For the AA7075 as a function of SiC reinforcement percentual, the crystallite size, micro deformation, particle size, morphologies, and chemical composition presented like AA7075 milled 480 min, independently if no reinforcement was used or if the SiC reinforces percentual was used until 5 percent.
4- The best structural refinement result was achieved when 10 percent of SiC reinforcement was applied AA7075 milling 480 min (25nm to crystallite size, 0.16 percent to micro deformation, and 9μm to particle size).

5. Acknowledgments

This work has been carried out under the projects: “Functional” - Partnership between the Federal University of Pernambuco and European Union’s Seventh Framework Programme for Research and “Aluminum Metal Matrix Composite Ceramic Particulate Reinforcement” of the Federal Rural University of Pernambuco, National Council for Scientific and Technological Develop (CNPq) – Brazil and Pernambuco Science and Technology Support Foundation (FACEPE)- Brazil.

6. References

1. Imran M, Khan ARA, Megeri S, Sadik S. Study of hardness and tensile strength of Aluminum-7075 percentage varying reinforced with graphite and bagasse-ash composites. Resource-Efficient Technologies. 2016;2(2):81-8.
2. Manoja M, Jinub GR, Muthuramalingamc T, Singhd RLB. Synthetization and investigation on mechanical characteristics of aluminum alloy 7075 with TiB2 composite. J Ceram Process Res. 2021;4:475-81.
3. Thirumalvalavam S, Senthilkumar N. Evaluation of mechanical properties of aluminium alloy (LM25) reinforced with fused silica matrix composite. Indian J Eng Mater Sci. 2019;26:59-66.
4. Subramaniam B, Natarajan B, Kaliyaperumal B, Chelladurai SJS. Investigation on mechanical properties of aluminum 7075 - boron carbide - coconut shell fly ash reinforced hybrid metal matrix composites. Overseas Foundry. 2018;15(6):449-56.
5. Barakat WS, Habba MIA, Ibrahim A, Fathy A, Elkady OA. The effect of Cu coated Al_2O_3 particle content and densification methods on the microstructure and mechanical properties of Al matrix composites. J Mater Res Technol. 2023;24:6908-22.
6. Ahmadian H, Sadoun AM, Fathy A, Zhou T. Utilizing a unified conceptual dynamic model for prediction of particle size of dual-matrix nanocomposites during mechanical alloying. Powder Technol. 2023;418:118291.

7. Sadoun AM, Mohamed MM, El Sayed, Meselhy AF, El-Kady OA. Effect of nano Al_2O_3 coated Ag reinforced Cu matrix nanocomposites on mechanical and tribological behavior synthesis by P/M technique. J Compos Mater. 2020;9(3):4485-93.
8. Najjar IMR, Sadoun AM, Abd Elaziz M, Abdallah AW, Fathy A, Elsheikh AH. Predicting kerf quality characteristics in laser cutting of basalt fibers reinforced polymer composites using neural network and chimp optimization. Alex Eng J. 2022;61(12):11005-18.
9. Sadoun AM, Najjar IMR, Alsoruji GS, Abd-Elwahed MS, Elaziz MA, Fathy A. Utilization of improved machine learning method based on artificial hummingbird algorithm to predict the tribological behavior of Cu-Al_2O_3 nanocomposites synthesized by in situ method. Mathematics. 2022;12(8):1266.
10. Sadoun AM, Meselhy AF, Abdallah AW. Microstructural, mechanical and wear behavior of electroless assisted silver coated Al_2O_3–Cu nanocomposites. Mater Chem Phys. 2021;266:124562.
11. Sadoun AM, Ibrahim A, Abdallah AW. Fabrication and evaluation of tribological properties of Al_2O_3 coated Ag reinforced copper matrix nanocomposite by mechanical alloying. J Asian Ceramic Societies. 2020;8(4):1228-38.
12. El-Wazery MS, El-Desouky AR, Hamed OA, Fathy A, Mansour NA. Electrical and mechanical performance of zirconia-nickel functionally graded materials. Int J Eng. 2013;26(4):375-82.
13. Shehata F, Abdelhameed M, Fathy A, Elmahdy M. Preparation and characteristics of Cu-Al_2O_3 nanocomposite. Open J Met. 2011;1(2):25-33.
14. Sadoun AM, Najjar IMR, Fathy A, Abd Elaziz M, Al-Ganess MAA, Abdallah AW, et al. An enhanced Dendritic Neural Algorithm to predict the wear behavior of alumina coated silver reinforced copper nanocomposites. Alex Eng J. 2023;65:809-23.
15. Najjar IMR, Sadoun AM, Fathy A, Abdallah AW, Elaziz MA, Elmahdy M. Prediction of tribological properties of alumina-coated, silver-reinforced copper nanocomposites using long short-term model combined with golden jackal optimization. Lubricants. 2022;10(11):277.
16. Chen HB, Tao K, Yang B, Zhang J. Nanostructured Al-Zn-Mg-Cu alloy synthesized by cryomilling and spark plasma sintering. Trans Nonferrous Met Soc China. 2009;19(5):1110-5.
17. Renk O, Pippan R. Saturation of grain refinement during severe plastic deformation of single-phase materials: reconsiderations, current status and open questions. Mater Trans. 2019;7(7):1270-82.
18. Segal V. Review: modes and processes of Severe Plastic Deformation (SPD). Materials. 2018;11(7):1175.
19. Lee HH, Yoon JI, Kim HS. Single-roll angular-rolling: a new continuous severe plastic deformation process for metal sheets. Scr Mater. 2018;146:204-7.
20. Velázquez-Carrillo OA, García-Pastor FA. Thermal stability of microstructure, mechanical properties, formability parameters and crystallographic texture in an Al-7075 alloy processed by accumulative roll bonding. J Mater Res Technol. 2021;11:2208-20.
21. Sabirov I, Murashkin MY, Valiev RZ. Nanostructured aluminum alloys produced by severe plastic deformation: new horizons in development. Mater Sci Eng A. 2013;560:1-24.
22. Zhou P, Deng L, Xie J, Liang D, Zheng L. A study about Fe-Ni mechanical alloying process by dry and wet method. J Electron Sci Technol China. 2005;3:2.
23. Kocsor L, Kovács L, Bencs L, Kolonits T, Lengyel K, Bazsó G, et al. Lithium oxide loss of lithium niobate nanocrystals during high-energy ball-milling. J Alloys Compd. 2022;909:164713.
24. Chen C, Li F, Han W, Lu T, Li P, Cui Q, et al. Thermally stable Al conductor prepared from Al powder with a low oxygen content. Mater Sci Eng A. 2021;813:141174.
25. Carreño-Gallardo C, Estrada-Guel I, López-Meléndez C, Martínez-Sánchez R. Dispersion of silicon carbide nanoparticles in a AA2024 aluminum alloy by a high-energy ball mill. J Alloys Compd. 2014;586:S68-72.
26. Gauthier M, Mazouzi D, Reyter D, Lestriez B, Moreau P, Guyomard D, et al. A low-cost and high-performance ball-milled Si-based negative electrode for high-energy Li-ion batteries. Energy Environ Sci. 2013;6(7):2145-55.
27. Deaquino-Lara R, Estrada-Guel I, Hinojosa-Ruiz G, Flores-Campos R, Herrera-Ramírez JM, Martínez-Sánchez R. Synthesis of aluminum alloy 7075-graphite composites by milling process and hot extrusion. J Alloys Compd. 2011;509S:284-9.
28. Suryanarayana C. Mechanical alloying and milling. Prog Mater Sci. 2001;46(1-2):1-184.
29. Burmeister CF, Kwade A. Process engineering with planetary ball mills. Chem Soc Rev. 2013;42(18):7660-7.
30. Lv H, Zhao X, Niu H, He S, Tang Z, Wu F, et al. Ball milling synthesis of covalent organic framework as a highly active photocatalyst for degradation of organic contaminants. J Hazard Mater. 2019;369:494-502.
31. Zepon G, Leiva DR, Strozi RB, Bedoch A, Figueroa SJC, Ishikawa TT, et al. Hydrogen-induced phase transition of $MgZrTiFe_{0.5}Co_{0.5}Ni_{0.5}$ high entropy alloy. Int J Hydrogen Energy. 2018;43(3):1702-8.
32. Soares L, Dal-Bó AG, Bernardin AM. Use of enameling wastewater in the wet milling process for 'monoporosa'tile composition. Cleaner Eng Technol. 2021;5:100338.
33. Syugaev AV, Maratkanova AN, Yazovskikh KA, Makarova AA, Bazhenov VV. Interface structure and corrosion protection of hybrid particles prepared via surfactant- and silica-assisted wet ball milling. Results Surf Interfaces. 2022;8:100079.
34. Suryanarayana C, Norton MG. X-ray diffraction: a practical approach. New York: Plenum Press; 1998.
35. Del Rio Castillo AE, Pellegrini V, Ansaldo A, Ricciardella F, Sun H, Marasco L, et al. High-yield production of 2D crystals by wet-jet milling. Mater Horiz. 2018;5(5):890-904.
36. Malamatari M, Taylor KMG, Malamataris S, Douroumis D, Kachrimanis K. Pharmaceutical nanocrystals: production by wet milling and applications. Drug Discov Today. 2018;23(3):534-47.
37. Le Caër G, Ziller T, Delcroix P, Bellouard C. Mixing of iron with various metals by high-energy ball milling of elemental powders mixtures. Hyperfine Interact. 2000;130(1-4):45-70.
38. Chelgani SC, Parian M, Semsari Parapari P, Ghorbani Y, Rosenkranz J. A comparative study on the effects of dry and wet grinding on mineral flotation separation: a review. J Mater Res Technol. 2019;8(5):5004-11.
39. Patil NA, Pedapati SR, Marode RV. Wear analysis of friction stir processed AA7075-SiC-graphite hybrid surface composites. Lubricants. 2022;10(10):267.
40. Lira HM, Rodrigues PR, Araujo OO Fo, Gonzales CH, Urtiga SP Fo. Nanostructured Al powder obtained by high energy ball milling at ambient and cryogenic temperatures. Mater Sci Forum. 2014;802:125-9.
41. Thomas S, Kalarikkal N, Abraham AR. Design, fabrication and characterization of multifunctional nanomaterials. 1st ed. Amsterdam: Elsevier; 2021. p. 319-41.
42. Gubicza J, Kassem M, Ribárik G, Ungár T. The microstructured of mechanically alloyed Al-Mg determined by X-ray diffraction peak profile analysis. Mater Sci Eng A. 2004;372(1-2):115-22.
43. Monshi A, Foroughi MR, Monshi MR. Modified Scherrer equation to estimate more accurately nano-crystallite size using XRD. World Journal of Nano Science and Engineering. 2012;2(3):154-60.
44. Svensson DN, Messing I, Barron J. An investigation in laser diffraction soil particle size distribution analysis to obtain compatible results with sieve and pipette method. Soil Tillage Res. 2022;223:105450.
45. ISO: International Organization for Standardization. ISO 13320: particle size analysis-laser diffraction methods. Geneva: ISO; 2020.
46. ISO: International Organization for Standardization. ISO 9672-1: representation of results of particle size analysis. Part 1: graphical representation. Geneva: ISO; 2001.
47. ISO: International Organization for Standardization. ISO 9672-2. ISO 9672-2: representation of results of particle size

analysis. Part 2: calculation of average particle sizes/diameters and moments from particle size distributions. Geneva: ISO; 2001.
48. Fernández H, Ordoñez S, Pesenti H, González RE, Leoni M. Microstructure homogeneity of milled aluminum A356–Si3N4 metal matrix composite powders. J Mater Res Technol. 2019;8(3):2969-77.
49. Nouri A, Hodgson PD, Wen C. Effect of ball-milling time on the structural characteristics of biomedical porous Ti-Sn-Nb alloy. Mater Sci Eng C. 2011;31(5):921-8.
50. Salah N, Habib SS, Khan ZH, Memic A, Azam A, Alarfaj E, et al. High energy ball milling technique for ZnO nanoparticles antibacterial material. Int J Nanomedicine. 2011;6:863-9.
51. Soares E, Bouchonneau N, Alves E, Alves K, Araújo O Fo, Mesguich D, et al. Microstructure and mechanical properties of AA7075 aluminum alloy fabricated by Spark Plasma Sintering (SPS). Materials. 2021;14(2):430.
52. Estrada-Ruiz RH, Flores-Campos R, Treviño-Rodríguez GA, Herrera-Ramírez JM, Martínez-Sánchez R. Wear resistance analysis of the aluminum 7075 alloy and the nanostructured aluminum 7075 - silver nanoparticles composites. J Min Metall Sect B Metall. 2016;52:163-70.
53. Nariki S, Seo KJ, Sakai N, Murakami M. Influence of the size of Gd211 starting powder on the critical current density of Gd-Ba-Cu-O bulk superconductor. Supercond Sci Technol. 2000;13(6):778-84.
54. Jung HJ, Sohn Y, Sung HG, Hyun HS, Shin WG. Physicochemical properties of ball milled boron particles: dry vs. wet ball milling process. Powder Technol. 2015;269:548-53.
55. Ji YY, Xu Y, Zhang B, Behnamian Y, Xia D, Hu W. Xu Yz, Zhang BB, Behnamian Y, Xia DH, Hu WB. Review of micro-scale and atomic-scale corrosion mechanisms of second phases in aluminum alloys. Trans Nonferrous Met Soc China. 2021;31(11):3205-27.
56. Bamberg P, Gintrowski G, Liang Z, Schiebahn A, Reisgen U, Precoma N, et al. Development of a new approach to resistance spot weld AW-7075 aluminum alloys for structural applications: an experimental study – Part 1. J Mater Res Technol. 2021;15:5569-81.